Fast high-resolution nuclear magnetic resonance spectroscopy through indirect zero-quantum coherence detection in inhomogeneous fields*

Ke Han-Ping(柯汉平), Chen Hao(陈 浩), Lin Yan-Qin(林雁勤)†, Wei Zhi-Liang(韦芝良), Cai Shu-Hui(蔡淑惠)‡, Zhang Zhi-Yong(张志勇), and Chen Zhong(陈 忠)

Department of Electronic Science, Fujian Provincial Key Laboratory of Plasma and Magnetic Resonance, Xiamen University, Xiamen 361005, *China*

(Received 16 September 2013; revised manuscript received 19 November 2013; published online 10 April 2014)

In many cases, high-resolution nuclear magnetic resonance (NMR) spectra are virtually impossible to obtain by conventional nuclear magnetic resonance methods because of inhomogeneity of magnetic field and inherent heterogeneity of sample. Although conventional intramolecular zero-quantum coherence (ZQC) can be used to obtain high-resolution spectrum in inhomogeneous field, the acquisition takes rather long time. In this paper, a spatially encoded intramolecular ZQC technique is proposed to fast acquire high-resolution NMR spectrum in inhomogeneous field. For the first time, the gradient-driven decoding technique is employed to selectively acquire intramolecular ZQC signals. Theoretical analyses and experimental observations demonstrate that high-resolution NMR spectral information can be retrieved within several scans even when the field inhomogeneity is severe enough to erase most spectral information. This work provides a new way to enhance the acquisition efficiency of high-resolution intramolecular ZQC spectroscopy in inhomogeneous fields.

Keywords: nuclear magnetic resonance, intramolecular zero-quantum coherence, inhomogeneous magnetic fields, spatial encoding

PACS: 32.30.Dx, 82.56.–b **DOI:** 10.1088/1674-1056/23/6/063201

1. Introduction

High-resolution NMR is an important tool for molecular structure analysis. It delivers detailed molecular level information that shows subtle differences in the environment of various nuclei. In some cases, however, high-resolution NMR spectra are virtually impossible to obtain by conventional NMR methods because of the external field inhomogeneity or the internal heterogeneity of sample. Therefore, there is a great deal of interest in exploring high-resolution NMR techniques in inhomogeneous fields.

Many methods have been proposed to retrieve chemical shift information in inhomogeneous B_0 field. For example, one can compensate for the inhomogeneous B_0 field by a matched radio-frequency (RF) field.[1] One of the earliest and still most widely used methods is a spin echo that can refocus the phase accumulated by inhomogeneous B_0 field, demonstrate J-couplings, but completely eliminate chemical shift information.[2] A Fourier synthesis algorithm has been proposed to design phase-compensating RF pulses and pulsed-field gradients to obtain high-resolution spectra in spatially dependent inhomogeneous fields.[3] Many methods based on intermolecular multiple-quantum coherences (iMQCs), which have special properties,[4,5] have also been designed to acquire high-resolution NMR spectra in inhomogeneous and unstable fields.[6,7] A high-resolution two-dimensional (2D) J-resolved spectroscopic technique in inhomogeneous fields with two scans was proposed in 2011 based on intermolecular zero-quantum coherence (iZQC).[8] It is well known that the evolution of ZQC is insensitive to magnetic field inhomogeneity. Several high-resolution methods have been designed based on ZQC. Recently, high-resolution ^{1}H NMR spectra from rat brain *in vivo* under small field inhomogeneity was obtained via ZQC.[9,10] However, the long acquisition time is an obstacle since a high-resolution one-dimensional (1D) spectrum needs 2D acquisition.

Reducing the 2D NMR acquisition time is an important research topic in the NMR community. Many methods have been designed to obtain 2D NMR spectra as quickly as possible. For example, according to the optimization of the delays and pulse flip angles, Schanda and Brutscher[11] proposed a heteronuclear multiple quantum coherence (HMQC) sequence (SOFAST-HMQC) to acquire a 2D spectrum of protein sample in a few seconds. Linear prediction (LP)[12] and projection reconstruction (PR)[13] can use a small number of t_1 increments to construct the whole 2D FID signals. Some unconventional sampling schemes, such as radial sampling, concentric ring sampling, and sparse sampling have also been proposed.[14–18] In addition, the filter diagonalization method (FDM)[19] and Hadamard spectroscopy[20–22] can effectively reduce the duration of indirect dimension. Recently, Frydman *et al.*[23,24]

*Project supported by the National Natural Science Foundation of China (Grant Nos. 11275161 and 11105114).

†Corresponding author. E-mail: linyq@xmu.edu.cn

‡Corresponding author. E-mail: shcai@xmu.edu.cn

© 2014 Chinese Physical Society and IOP Publishing Ltd

proposed an ultrafast 2D NMR technique to enable the acquisition of a 2D NMR spectrum within a single scan. In this so-called "ultrafast 2D NMR" technique, the usual t_1 encoding is replaced by a spatial encoding, which is decoded during the detection period by an echo planar imaging (EPI) detection scheme. The ultrafast method has been successfully used in many NMR applications, including COSY,[25–27] TOCSY,[23,28–30] J-resolved spectroscopy,[31,32] HSQC,[23,28] HMQC,[33] HMBC,[34,35] and DOSY.[33]

In this study, we present an approach for high-resolution NMR spectra in inhomogeneous fields via an intramolecular ZQC technique and a spatially encoded technique. A high-resolution NMR spectrum can be acquired in a few seconds, despite a large range of magnetic field inhomogeneity.

2. Theoretical formalism

The pulse sequence is shown in Fig. 1(b). Instead of using the conventional preparation module 90°–TE–180°–TE–90°, we use the module 90°–TE–180°–TE–45° because it can eliminate all of the resonances from uncoupled spin systems ($TE \approx 1/4J$ in this study).[9] The conventional preparation module brings all uncoupled spin-systems to the longitudinal axis, where they cannot be differentiated from ZQCs. In fact, the uncoupled spin systems will be located in the (0, ω_2) midline. Note that the utilization of 45° RF pulse flip angle leads to 50% signal loss.[9,10] The symmetric gradient $G_{\rm A}$ is used to erase the frequency deviation, chemical shift, and magnetic field inhomogeneity. The gradient G_S in Fig. 1(b) is used to select the desired coherence transfer pathway, and $G_{\rm E}$ and $G_{\rm D}$ are the encoding and decoding gradients, respectively. The WURST adiabatic pulse has a duration of $\tau_{\rm ad}$. The gradient $G_{\rm P}$ prior to acquisition is adjusted to set the middle of chemical shift range to be in the middle of detection period $\tau_{\rm D}$. A significant part of the longitudinal magnetization and all of the longitudinal relaxation (T_1)-recovered magnetizations present during the spatially encoded period are removed through the magnetic field crusher gradients $G_{\rm B}$ and $G_{\rm C}$.

Without loss of generality, we consider a sample consisting of an AX spin-1/2 system, where A and X represent I and S spins with internal frequency shifts Ω_I and Ω_S, and a scalar coupling constant J, respectively. The effective sample length is L (the z coordinate ranges from $-L/2$ to $L/2$). All of the RF pulses are applied along the x direction, except for the $\pi/4$ pulse in the y direction. Ignoring the effects of relaxation, diffusion, radiation damping, and crusher gradients, we will see how the spins evolve under the pulse sequence in Fig. 1(b). The reduced density operator $\sigma_{\rm eq}$ for the two protons in each molecule in the initial thermal equilibrium state within the high-temperature approximation can be given by

$$\sigma_{\rm eq} = I_z + S_z, \tag{1}$$

where the Boltzmann factor has been omitted for clarity. I_z and S_z represent the longitudinal components of I and S spins, respectively. Only I is considered in the following deduction because S is similar to I in an AX spin-1/2 system.

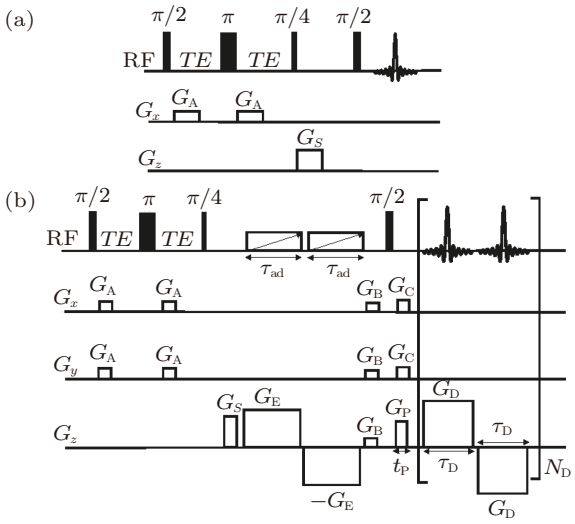


Fig. 1. Pulse sequences for high-resolution NMR spectra in arbitrarily inhomogeneous fields. (a) Conventional pulse sequence for high-resolution NMR spectra through intramolecular ZQC; (b) pulse sequence for fast high-resolution NMR spectra through intramolecular ZQC.

The first non-selective 90° RF pulse excites the longitudinal magnetization into the transverse plane. After the spin echo module of TE–180°–TE, the frequency deviation, chemical shift, and magnetic field inhomogeneity are refocused. Just before the $\pi/4$ RF pulse, the spin system can be described by the reduced density operator as

$$\sigma_1 = -\left(I^+ + I^-\right) S_z. \tag{2}$$

The non-selective 45° RF pulse turns Eq. (2) into

$$\sigma_2 = -\frac{1}{4}\left(I^+ + I^- - 2I_z\right)\left(S^+ + S^- + 2S_z\right). \tag{3}$$

Due to the pathway transfer selective gradient $G_{\rm S}$, only ZQC signals can finally be observed. Additionally, I_zS_z is omitted because it cannot be detected during detection period. The observable part of the reduced density operator is

$$\sigma_3 = -\frac{1}{4}\left(I^+S^- + I^-S^+\right). \tag{4}$$

Only I^+S^- is considered in the following deduction because I^-S^+ is similar to I^+S^-. Due to the existence of the field gradients $\pm G_{\rm E}$, the π chirp pulses sequentially excite the sample layer by layer along the z axis. During the first spatially encoded block (comprising a linearly swept adiabatic refocusing pulse in the presence of a gradient $G_{\rm E}$), I^+S^- is subjected to spatial encoding. At the end of this block, the reduced density operator can be given as

$$\sigma_4 = I^-S^+\left[\cos\left(\pi J\tau_{\rm ad}\right) + 2{\rm i}S_z\sin\left(\pi J\tau_{\rm ad}\right)\right]$$

$$\times [\cos(\pi J\tau_{\rm ad}) - 2{\rm i}I_z \sin(\pi J\tau_{\rm ad})]$$
$$\times \exp\left\{{\rm i}\frac{1}{R}(\Omega_S - \Omega_I)[\Omega_S + \Omega_I + 2(\gamma G_{\rm E} z + \gamma\Delta B - O_{\rm ctr})]\right\}, \quad (5)$$

where $O_{\rm ctr}$ is the center of frequency bandwidth excited by the 180° adiabatic chirp RF pulse, and the sweep rate $R = \Delta\omega_{\rm ad}/\tau_{\rm ad}$, given by the ratio between the sweep width $\Delta\omega_{\rm ad}$ and the duration $\tau_{\rm ad}$ of the adiabatic pulse, ΔB is the distribution of magnetic field inhomogeneity, γ is the gyromagnetic ratio of proton. After the second spatially encoded block, the reduced density operator is updated to

$$\begin{aligned}\sigma_5 &= I^+S^-[\cos(2\pi J\tau_{\rm ad}) - 2{\rm i}S_z\sin(2\pi J\tau_{\rm ad})] \\ &\times [\cos(2\pi J\tau_{\rm ad}) + 2{\rm i}I_z\sin(2\pi J\tau_{\rm ad})] \\ &\times \exp\left[{\rm i}\gamma G_{\rm E} z\frac{4(\Omega_S - \Omega_I)}{R}\right]. \end{aligned} \quad (6)$$

The last 90° RF pulse completes the transfer of ZQC to directly detectable single-quantum coherence (SQC) signals

$$\begin{aligned}\sigma_6 &= \left(\frac{I^+ + I^-}{2} + {\rm i}I_z\right)\left(\frac{S^+ + S^-}{2} - {\rm i}S_z\right) \\ &\times \left[\cos(2\pi J\tau_{\rm ad}) - (S^+ - S^-)\sin(2\pi J\tau_{\rm ad})\right] \\ &\times \left[\cos(2\pi J\tau_{\rm ad}) + (I^+ - I^-)\sin(2\pi J\tau_{\rm ad})\right] \\ &\times \exp\left[{\rm i}\gamma G_{\rm E} z\frac{4(\Omega_S - \Omega_I)}{R}\right]. \end{aligned} \quad (7)$$

The echo planner spectroscopic imaging (EPSI) like detection module is utilized to repetitiously read out the resonances determined echoes. For convenience of analysis, a running variable n is defined to denote the order of different lobes of alternating gradients. In the $(2n-1)$ lobe of gradient, the detectable signals can be expressed as

$$\begin{aligned}\sigma_{\rm obs} &= \frac{1}{4}\Big\{I^-\,{\rm e}^{{\rm i}(\Omega_I + \gamma\Delta B)[(2n-2)\tau_{\rm D} + t_{\rm D}]} \\ &- S^-\,{\rm e}^{{\rm i}(\Omega_S + \gamma\Delta B)[(2n-2)\tau_{\rm D} + t_{\rm D}]}\Big\} \\ &\times \sin[\pi J(2n-2)\tau_{\rm D} + \pi J t_{\rm D}] \\ &\times \exp\left\{{\rm i}\gamma G_{\rm E} z\left[\frac{4(\Omega_S - \Omega_I)}{R} + \frac{G_{\rm P}}{G_{\rm E}}t_{\rm P} + \frac{1}{G_{\rm E}}\int_0^{t_{\rm D}} G_{\rm D}(t)\,{\rm d}t\right]\right\}\cos^2(2\pi J\tau_{\rm ad}). \end{aligned} \quad (8)$$

Since the sample length along the z orientation is much larger than the length along the x or y direction, the field inhomogeneity along the z direction generally constitutes the major part of the total inhomogeneity. Furthermore, if the field inhomogeneity is linear, namely

$$\gamma\Delta B \approx \gamma G_{\Delta B} z, \quad (9)$$

where $G_{\Delta B}$ is the intensity of the field gradient originating from the inhomogeneous field, equation (8) can be rewritten as

$$\begin{aligned}\sigma_{\rm obs} &= \frac{1}{4}\Big\{I^-\,{\rm e}^{{\rm i}\Omega_I[(2n-2)\tau_{\rm D} + t_{\rm D}]} - S^-\,{\rm e}^{{\rm i}\Omega_S[(2n-2)\tau_{\rm D} + t_{\rm D}]}\Big\} \\ &\times \sin[\pi J(2n-2)\tau_{\rm D} + \pi J t_{\rm D}] \\ &\times \exp\left\{{\rm i}\gamma G_{\rm E} z\left\{\frac{4(\Omega_S - \Omega_I)}{R} + \frac{G_{\rm P}}{G_{\rm E}}t_{\rm P} + \frac{1}{G_{\rm E}}\int_0^{t_{\rm D}} G_{\rm D}(t)\,{\rm d}t + \frac{G_{\Delta B}}{G_{\rm E}}[(2n-2)\tau_{\rm D} + t_{\rm D}]\right\}\right\} \\ &\times \cos^2(2\pi J\tau_{\rm ad}), \end{aligned} \quad (10)$$

where $t_{\rm D}$ denotes the time running from the beginning of each positive lobe of the alternating decoding gradients.

The observed signal can be calculated as

$$\begin{aligned}M_+ &= M_0 \times \int_{-L/2}^{L/2} {\rm Tr}\left[(I^+ + S^+)\cdot\sigma_{\rm obs}\right]{\rm d}z \\ &= \frac{M_0}{4}\times\int_{-L/2}^{L/2}\Big\{{\rm e}^{{\rm i}\Omega_I[(2n-2)\tau_{\rm D} + t_{\rm D}]} - {\rm e}^{{\rm i}\Omega_S[(2n-2)\tau_{\rm D} + t_{\rm D}]}\Big\} \\ &\times \sin[\pi J(2n-2)\tau_{\rm D} + \pi J t_{\rm D}] \\ &\times \exp\left\{{\rm i}\gamma G_{\rm E} z\left\{\frac{4(\Omega_S - \Omega_I)}{R} + \frac{G_{\rm P}}{G_{\rm E}}t_{\rm P} + \frac{1}{G_{\rm E}}\int_0^{t_{\rm D}} G_{\rm D}(t)\,{\rm d}t + \frac{G_{\Delta B}}{G_{\rm E}}[(2n-2)\tau_{\rm D} + t_{\rm D}]\right\}\right\} \\ &\times \cos^2(2\pi J\tau_{\rm ad})\,{\rm d}z \\ &= \frac{M_0}{4}L\Big\{{\rm e}^{{\rm i}\Omega_I[(2n-2)\tau_{\rm D} + t_{\rm D}]} - {\rm e}^{{\rm i}\Omega_S[(2n-2)\tau_{\rm D} + t_{\rm D}]}\Big\} \\ &\times \sin[\pi J(2n-2)\tau_{\rm D} + \pi J t_{\rm D}] \\ &\times \sin c\left\{\frac{\gamma G_{\rm E} L}{2}\left[\frac{4(\Omega_S - \Omega_I)}{R} + \frac{G_{\rm P}}{G_{\rm E}}t_{\rm P} + \frac{G_{\rm D}}{G_{\rm E}}t_{\rm D} + \frac{G_{\Delta B}}{G_{\rm E}}(2n-2)\tau_{\rm D} + \frac{G_{\Delta B}}{G_{\rm E}}t_{\rm D}\right]\right\}\cos^2(2\pi J\tau_{\rm ad}), \end{aligned} \quad (11)$$

where M_0 is the equilibrium magnetization per unit volume of I or S spin.

According to Eq. (10), an echo will appear at the moments when

$${\rm i}\gamma G_{\rm E} z\left\{\frac{4(\Omega_S - \Omega_I)}{R} + \frac{G_{\rm P}}{G_{\rm E}}t_{\rm P} + \frac{G_{\rm D}}{G_{\rm E}}t_{\rm D} + \frac{G_{\Delta B}}{G_{\rm E}}[(2n-2)\tau_{\rm D} + t_{\rm D}]\right\} = 0. \quad (12)$$

The signals in the resulting 2D spectrum will then be located at $(\Omega_{\rm S} - \Omega_I, \Omega_I)$ and $(\Omega_S - \Omega_I, \Omega_S)$. Similarly, the signals evolving from S spin will be located at $(\Omega_I - \Omega_S, \Omega_I)$ and $(\Omega_I - \Omega_S, \Omega_S)$ in the resulting 2D spectrum. This shows that the resonances in the indirect ($F1$) dimension appear at positions that are determined by the frequency difference between the coupled spins while the resonances in the direct ($F2$) dimension appear at their respective Larmor frequencies.

With the running variable $t_{\rm D}$, a series of echoes corresponding to chemical shift intervals can be detected. The extreme chemical shift intervals within the observable frequency

ranges are

$$\begin{cases} \dfrac{4(\Delta\Omega)_{\max}}{R}+\dfrac{G_{\rm P}}{G_{\rm E}}t_{\rm P}+\dfrac{G_{\rm D}}{G_{\rm E}}\times 0 \\ \quad +\dfrac{G_{\Delta B}}{G_{\rm E}}\left[(2n-2)\tau_{\rm D}+0\right]=0, \\ \dfrac{4(\Delta\Omega)_{\min}}{R}+\dfrac{G_{\rm P}}{G_{\rm E}}t_{\rm P}+\dfrac{G_{\rm D}}{G_{\rm E}}\tau_{\rm D} \\ \quad +\dfrac{G_{\Delta B}}{G_{\rm E}}\left[(2n-2)\tau_{\rm D}+\tau_{\rm D}\right]=0. \end{cases} \tag{13}$$

The spectral width in the $F1$ dimension can be taken as the frequency range of the series of echoes, namely

$$SW_{F1}=(\Delta\Omega)_{\max}-(\Delta\Omega)_{\min}=\frac{G_{\rm D}+G_{\Delta B}}{4G_{\rm E}}R\tau_{\rm D}. \tag{14}$$

For the same chemical shift interval of $\Delta\Omega$, the moment to reach the summit of echo is given from Eq. (12) as follows:

$$t_{\rm e}=\frac{1}{G_{\rm D}+G_{\Delta B}}\left[\frac{4\Delta\Omega G_{\rm E}}{R}+G_{\rm P}t_{\rm P}+(2n-2)G_{\Delta B}\tau_{\rm D}\right]. \tag{15}$$

It can be inferred from Eq. (15) that $t_{\rm e}$ varies with the running variable n, suggesting that the series of $\Delta\Omega$-determined echoes experiences a shift of $\Delta t_{\rm e}=2G_{\Delta B}\tau_{\rm D}/(G_{\rm D}+G_{\Delta B})$ between every adjacent odd or even lobe of the gradients. Since the echoes shift with the running variable n, the spectral width needed to cover all resonances ascends.

The indirect dimension is directly related to frequency, indicating that Fourier transformation (FT) is no longer required to obtain frequency information, and the resolution in $F1$ dimension can be calculated through a simple conversion as

$$\Delta\nu_{\rm F1}=1.21SW_{\rm F1}\frac{\Delta t}{\tau_{\rm D}}=\frac{0.605\pi\Delta\omega_{\rm ad}}{\gamma G_{\rm E}L\tau_{\rm ad}}, \tag{16}$$

where Δt is the first positive zero-passing point of the sinc function in Eq. (11).

3. Materials and methods

All of the experiments were performed at 298 K using a Varian NMR System 500 MHz spectrometer (Varian, Palo Alto, CA, USA), equipped with a 1.6-cm indirect detection probe with 3D gradient coils. In the conventional ZQC experiment, the phases for the first $\pi/2$ and the $\pi/4$ pulses (Fig. 1(a)) and the receiver were cycled as $(x, x, -x, -x)$, $(y, -y, y, -y)$, and $(x, -x, x, -x)$, respectively. The fast ZQC pulse sequence in Fig. 1(b) was used with an eight-step phase cycling scheme: the phases for the first $\pi/2$ and the $\pi/4$ pulses and the receiver were $(x, x, -x, -x, x, x, -x, -x)$, $(y, -y, y, -y, y, -y, y, -y)$, and $(x, -x, x, -x, x, -x, x, -x)$, respectively. The gradient strengths $G_{\rm B}$ and $G_{\rm C}$ took the opposite values in the first four steps and the next four steps to remove the significant part of the longitudinal magnetization and all of the T_1-recovered magnetizations present during the spatially encoded time, respectively.

Two samples were used to test the capability of the proposed pulse sequence. The first one was pure ethyl 3-bromopropionate ($BrCH_2^bCH_2^cCOOCH_2^aCH_3^d$) liquid, the second one was the mixture of 1-propyl alcohol ($CH_3^eCH_2^cCH_2^aOH$) and 2-butanone ($CH_3^dCH_2^bCOCH_3$) with a molar ratio of 2:1. For comparison, conventional ZQC spectra were also acquired using the pulse sequence shown in Fig. 1(a). The inhomogeneous field was created by de-shimming the Z1 coil or the X1 coil. In the conventional ZQC experiments, the same parameter settings were used in homogeneous and inhomogeneous fields. The pulse relaxation delay was 2 s, and 256 t_1 increments were acquired. For the first sample, the duration of $\pi/2$ RF pulse was 9.75 μs, with an RF power of 58 dB. The spectral widths of $F1$ and $F2$ dimensions were 5000 Hz and 4000 Hz, respectively. $TE=35.71$ ms. For the second sample, the duration of $\pi/2$ RF pulse was 9.9 μs, with an RF power of 58 dB. The spectral widths of $F1$ and $F2$ dimensions were 2500 Hz and 3000 Hz, respectively. $TE=34.22$ ms. The other parameters for both samples were as follows: $G_{\rm A}=2.93$ Gs/cm (1 Gs = 10^{-4} T), and $G_{\rm S}=13.67$ Gs/cm. The total acquisition time for a 2D spectrum was about 56 min.

In the fast ZQC experiments, the pulse relaxation delay was 5 s. $TE=35.71$ ms for the first sample, and $TE=34.22$ ms for the second sample. The WURST adiabatic pulse with 200-kHz sweep range was applied within 30 ms unless otherwise specified. In homogeneous field, $G_{\rm A}=0$ Gs/cm, and $N_{\rm D}=200$. For the first sample, the other experimental parameters were set as follows: $G_{\rm S}=9.77$ Gs/cm, $G_{\rm B}=37.5$ Gs/cm, $G_{\rm C}=0$ Gs/cm, $G_{\rm P}=-19.53$ Gs/cm, $t_{\rm P}=0.15$ ms, $G_{\rm E}=23.44$ Gs/cm, and $G_{\rm D}=39.06$ Gs/cm. $np1=900$, where $np1$ is the acquisition number during $\tau_{\rm D}$. For the second sample, the other experimental parameters were set as follows: $G_{\rm S}=-1.37$ Gs/cm, $G_{\rm B}=5.86$ Gs/cm, $G_{\rm C}=0$ Gs/cm, $G_{\rm P}=-9.77$ Gs/cm, $t_{\rm P}=0.20$ ms, $G_{\rm E}=39.06$ Gs/cm, $G_{\rm D}=39.06$ Gs/cm, and $np1=700$. In the inhomogeneous field created by de-shimming the Z1 coil (the line-width was 2000 Hz for the first sample and 1500 Hz for the second sample), $G_{\rm A}=-9.77$ Gs/cm, $G_{\rm S}=-27.34$ Gs/cm, $G_{\rm P}=-19.53$ Gs/cm, $G_{\rm D}=39.06$ Gs/cm, and $N_{\rm D}=200$. The other parameters were set as follows: $G_{\rm B}=13.67$ Gs/cm, $G_{\rm C}=-3.91$ Gs/cm, $t_{\rm P}=0.20$ ms, $G_{\rm E}=23.44$ Gs/cm, and $np1=700$ for the first sample; and, $G_{\rm B}=0$ Gs/cm, $G_{\rm C}=-5.86$ Gs/cm, $t_{\rm P}=0.10$ ms, $G_{\rm E}=35.16$ Gs/cm, and $np1=900$ for the second sample. In the inhomogeneous field with a line-width of 1000 Hz created by de-shimming the X1 coil (the line-width was 1000 Hz for the first sample and 300 Hz for the second sample), $G_{\rm A}=G_{\rm C}=0$ Gs/cm, $G_{\rm D}=39.06$ Gs/cm, and $N_{\rm D}=130$. The other parameters were set as follows: $G_{\rm B}=0$ Gs/cm, $G_{\rm S}=29.30$ Gs/cm, $G_{\rm P}=-9.77$ Gs/cm, $t_{\rm P}=0.30$ ms, $G_{\rm E}=23.44$ Gs/cm, and $np1=500$ for the first

sample. The sweep range of the adiabatic pulse was 160 kHz within 20 ms. For the second sample, $G_S = -13.67$ Gs/cm, $G_B = 5.86$ Gs/cm, $G_P = -19.53$ Gs/cm, $t_P = 0.10$ ms, $G_E = 39.06$ Gs/cm, and $np1 = 700$. The total acquisition time for a 2D spectrum was about 44 s.

To obtain a frequency-domain spectrum, the acquired time-domain data points were separated into two independent data sets related to $+G_D$ and $-G_D$ periods, respectively. Here, only the data acquired in $+G_D$ were considered. All the data were processed with the aid of our custom-written program in MATLAB 2010.

4. Results and discussion

The experimental results for the sample of ethyl 3-bromopropionate are shown in Fig. 2. While the resonances in the direct ($F2$) dimension of ZQC spectrum appear at their respective Larmor frequency sites, the resonances in the indirect ($F1$) dimension appear at the positions determined by the frequency difference between the spins involved in the zero-quantum transition (J-coupled spins). The average line-width of the conventional 1D high-resolution ^{1}H NMR spectrum is 3 Hz (Fig. 2(a)). In an homogeneous field, the average line-width of the peaks measured from the $F1$ projection spectrum is approximately 5 Hz (Fig. 2(b)) and 20 Hz (Fig. 2(c)). This indicates that our method cannot reach the resolution of conventional ^{1}H spectrum in homogeneous field. In the inhomogeneous fields (Figs. 2(d) and 2(g)), the average line-widths of the peaks measured from the $F1$ projection spectrum is approximately 45 Hz (Fig. 2(e)), 15 Hz (Fig. 2(h)), 23 Hz (Fig. 2(f)), and 22 Hz (Fig. 2(i). These results illustrate that

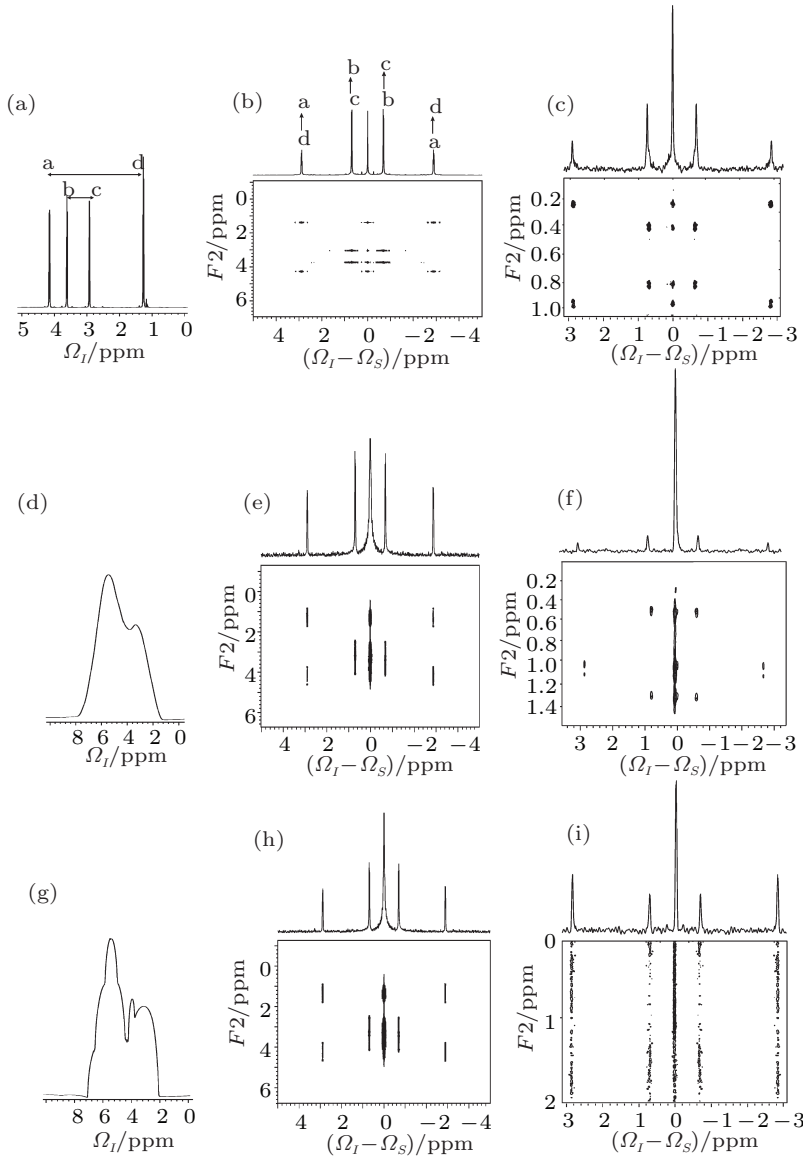


Fig. 2. 1D and 2D ZQC ^{1}H NMR spectra of ethyl 3-bromopropionate and their projection along the $F1$ dimension. (a), (d), (g): Conventional 1D spectrum acquired in a well-shimmed magnetic field (a), an inhomogeneous field with a line-width of 2000 Hz by de-shimming the Z1 coil (d), and an inhomogeneous field with a line-width of 1000 Hz by de-shimming the X1 coil (g); (b), (e), (h): 2D ZQC spectra acquired using the pulse sequence shown in Fig. 1(a) in the same fields as for panels (a), (d), and (g), and their projections along the $F1$ dimension respectively; (c), (f), (i): 2D ZQC spectra acquired using the pulse sequence shown in Fig. 1(b) in the same fields as for panels (a), (d), and (g), and their projections along the $F1$ dimension respectively. 2D spectra are presented in magnitude mode.

by tracking the difference of the precession frequencies between two spins, high-resolution spectral information can be obtained in inhomogeneous field. Since the axial peaks are much stronger than the cross peaks, they are used for resolution measurement. The resolution of the axial peak in the indirect dimension of the conventional ZQC spectrum may be degenerated due to t_1 ridge noise.[9] Therefore, the actual resolution of a conventional ZQC spectrum is generally higher than the given value when cross peaks are concerned. In our method, the spectral width of the $F1$ dimension is determined by Eq. (14), and the line-width of $F1$ spectrum is determined by Eq. (16). We can further improve the resolution by increasing the values of $G_{\rm E}$, $G_{\rm D}$, $\tau_{\rm D}$, and $\tau_{\rm ad}$ or reducing the value of $\Delta\omega_{\rm ad}$. Because the $F2$ dimension cannot provide useful information in inhomogeneous fields and will finally be discarded, we can raise the resolution of $F1$ spectrum by reducing the spectral width of $F2$ dimension. As a result of insufficient spectral width, the spectral lines may fold over and give incorrect chemical shifts. Moreover, due to the symmetry of the spectrum along the $F1$ dimension, we only acquired half of $F1$ dimension to improve the line-width of the $F1$ spectrum. The 2D ZQC spectra and their projections along the $F1$ dimension in Figs. 2(c), 2(f), and 2(i) were obtained by mirroring their related half-spectra.

The experimental results for the mixture of 1-propyl alcohol and 2-butanone are shown in Fig. 3. The average line-width of the conventional 1D high-resolution ^{1}H NMR spectrum is 3 Hz (Fig. 3(a)) in an homogeneous field. In the projection of 2D ZQC spectrum along the $F1$ dimension, the peak position is determined by the frequency difference between the J-coupled spins involved in the ZQC transfer. In an homogeneous field, the average line-widths of the peaks measured from the projection spectrum are approximately 5 Hz (Fig. 3(b)) and 20 Hz (Fig. 3(c)). In the two inhomogeneous fields (Figs. 3(d) and 3(g)), the average line-widths of the peaks measured from the projection spectrum are approximately 13 Hz (Figs. 3(e) and 3(h)), 23 Hz (Fig. 3(f)), and 22 Hz (Fig. 3(i)). These results give the same conclusions as those of Fig. 2.

The results of two samples show that the projections of fast 2D ZQC spectra along the indirect dimension indicate greatly improved spectral resolution compared with the projections along the direct dimension. Furthermore, the spectral

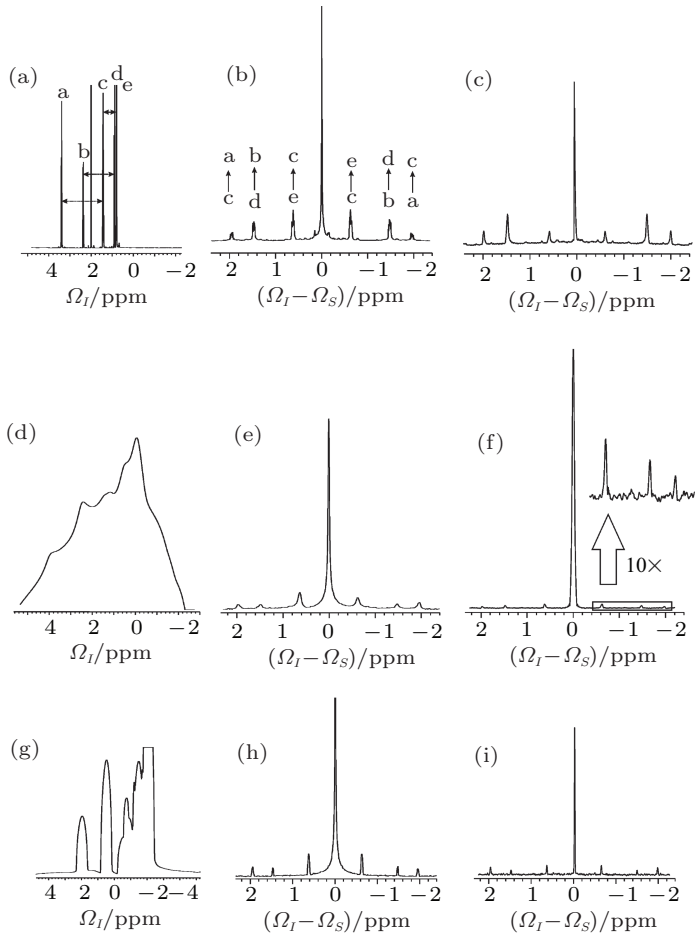


Fig. 3. 1D ^{1}H NMR spectra of 1-propyl alcohol and 2-butanone with a molar ratio of 2:1. (a), (d), (g): Conventional 1D spectrum acquired in a well-shimmed magnetic field (a), an inhomogeneous field with a line-width of 1500 Hz created by de-shimming the Z1 coil (d), and an inhomogeneous field with a line-width of 300 Hz created by de-shimming the X1 coil (g); (b), (e), (h): Projections of conventional 2D ZQC spectra acquired with the pulse sequence shown in Fig. 1(a) in the same field as for panels (a), (d), and (g) along the $F1$ dimension respectively; (c), (f), (i): Projections of 2D ZQC spectra acquired with the pulse sequence shown in Fig. 1(b) in the same field as for panels (a), (d), and (g) along the $F1$ dimension, respectively. The spectra are presented in magnitude mode.

resolution is independent of field homogeneity and is reproducible across different samples. Theoretically, our proposed scheme can give high-resolution one-dimensional spectra under arbitrary inhomogeneous magnetic field. However, it should be noted that the resolution may degenerate in cases where nonlinear field inhomogeneities exist in the encoding and decoding orientations.

Although the spectral resolution in the indirect dimension is greatly increased compared with the direct dimension, there are some factors influencing the spectral resolution in the indirect dimension. Firstly, the spectra are present in absolute value mode. A phase-sensitive display would allow a higher spectral resolution, but only when the dispersive component is minimized by optimizing the preparation time TE. Secondly, the (phase-sensitive) line-width in the indirect dimension is proportional to the ZQC transverse relaxation rate, which is generally faster than the relaxation rate of the corresponding SQC, leading to broader spectral lines. Thirdly, since the 2D resonances appear at the positions of chemical shift differences, rather than absolute chemical shifts, the effective spectral dispersion range has decreased.[9] Finally, the lower spectral resolution is an intrinsic limitation of spatially encoded methods.

As figures 2 and 3 show, the spectra acquired with our method have lower signal-to-noise ratio (SNR). There are several reasons for this. Firstly, the t_1-noise is not negligible. As a result, the apparent noise level increases compared with those of the 1D spectra. Secondly, the efficiency of generating and detecting ZQC is 25% of SQC at best.[9] More importantly, the spatially encoded technique itself causes lower SNR. Per scan, the ultrafast 2D NMR suffers an about $\sqrt{2N_1}$ penalty in its SNR vis-a-vis conventional NMR, where N_1 is the number of spectral elements in the single-scan ultrafast experiment along the indirect dimension. This is arguably the main handicap of the spatially encoded technique.[36] According to the spatially encoded principle, the SNR is inversely proportional to $\sqrt{\gamma G_{\mathrm{D}} L}$. The amplitude of decoding gradient G_{D} is determined by the spectral widths of indirect (SW_1) and direct (SW_2) dimensions ($G_{\mathrm{D}} = 2CSW_1SW_2/\gamma$).[37] Finally, the use of crusher gradients further debases the SNR. The SNRs are measured by dividing the intensity of the peak located at 0 ppm by the root-mean-square of noise ranging from -1.0 ppm to -2.5 ppm. The SNRs for spectra of Figs. 2(h) and 2(i) are 395 and 115, respectively.

In summary, we incorporate a ZQC transfer scheme into the spatially encoded technique to quickly obtain high-resolution 1H NMR spectra in an inhomogeneous field. This method can be potentially used for analyzing *in vivo* tissues and the *in vitro* real-time detection of heterogeneous chemical reaction systems. Compared with the conventional 2D ZQC method, this novel method opens a way to speed up high-resolution ZQC experiments in inhomogeneous fields. However, the issue of low SNR is still a critical problem. With the use of some currently available techniques, such as spin hyperpolarization and/or higher magnetic fields, this issue can be partially alleviated.

References

[1] Meriles C A, Sakellariou D, Heise H, Moule A J and Pines A 2001 *Science* **293** 82
[2] Hurlimann M D 2007 *J. Magn. Reson.* **184** 114
[3] Arthanari H, Frueh D, Wagner G, Pryor B and Khaneja N 2008 *J. Chem. Phys.* **128** 214503
[4] Chen S, Zhang X Q, Cai S H and Chen Z 2008 *Chin. Phys. B* **17** 915
[5] Zheng S K, Chen Z, Chen Z W and Zhong J H 2001 *Chin. Phys.* **10** 558
[6] Vathyam S, Lee S and Warren W S 1996 *Science* **272** 92
[7] Jiang B, Liu H L, Liu M L, Ye C H and Mao X 2008 *Chem. Phys.* **351** 33
[8] Lin Y L, Zhang Z Y, Cai S H and Chen Z 2011 *J. Am. Chem. Soc.* **133** 7632
[9] de Graaf R A, Rothman D L and Behar K L 2007 *J. Magn. Reson.* **187** 320
[10] de Graaf R A, Klomp D W, Luijten P R and Boer V O 2013 *Magn. Reson. Med.* 10.1002/mrm.24701
[11] Schanda P and Brutscher B 2005 *J. Am. Chem. Soc.* **127** 8014
[12] Stern A S, Li K B and Hoch J C 2002 *J. Am. Chem. Soc.* **124** 1982
[13] Kupce E and Freeman R 2004 *J. Am. Chem. Soc.* **126** 6429
[14] Kupce E and Freeman R 2005 *J. Magn. Reson.* **173** 317
[15] Coggins B E and Zhou P 2006 *J. Magn. Reson.* **182** 84
[16] Coggins B E and Zhou P 2007 *J. Magn. Reson.* **184** 207
[17] Coggins B E and Zhou P 2008 *J. Biomol. NMR* **42** 225
[18] Jiang B, Jiang X W, Xiao N, Zhang X, Jiang L, Mao X A and Liu M L 2010 *J. Magn. Reson.* **204** 165
[19] Mandelshtam V A, Taylor H S and Shaka A J 1998 *J. Magn. Reson.* **133** 304
[20] Kupce E and Freeman R 2003 *J. Magn. Reson.* **162** 300
[21] Kupce E and Freeman R 2003 *J. Magn. Reson.* **162** 158
[22] Kupce E and Freeman R 2003 *J. Magn. Reson.* **163** 56
[23] Frydman L, Lupulescu A and Scherf T 2003 *J. Am. Chem. Soc.* **125** 9204
[24] Frydman L, Scherf T and Lupulescu A 2002 *Proc. Nat. Acad. Sci. USA* **99** 15858
[25] Tal A, Shapira B and Frydman L 2005 *J. Magn. Reson.* **176** 107
[26] Wu C, Zhao M F, Cai S H, Lin Y L and Chen Z 2010 *J. Magn. Reson.* **204** 82
[27] Panek R, Granwehr J, Leggett J and Kockenberger W 2010 *Phys. Chem. Chem. Phys.* **12** 5771
[28] Pelupessy P 2003 *J. Am. Chem. Soc.* **125** 12345
[29] Herrera A, Fernandez-Valle E, Martinez-Alvarez R, Molero D, Pardo Z D, Saez E and Gal M 2009 *Angew. Chem. Int. Ed.* **48** 6274
[30] Zhang Z Y, Chen H, Wu C, Wu R, Cai S H and Chen Z 2013 *J. Magn. Reson.* **227** 39
[31] Giraudeau P and Akoka S 2007 *J. Magn. Reson.* **186** 352
[32] Roussel T, Giraudeau P, Rainey H, Akoka S and Cavassila S 2012 *J. Magn. Reson.* **215** 50
[33] Shrot Y and Frydman L 2008 *J. Magn. Reson.* **195** 226
[34] Gal M, Schanda P, Brutscher B and Frydman L 2007 *J. Am. Chem. Soc.* **129** 1372
[35] Giraudeau P, Shrot Y and Frydman L 2009 *J. Am. Chem. Soc.* **131** 13902
[36] Tal A and Frydman L 2010 *Prog. Nucl. Magn. Reson. Spectrosc.* **57** 241
[37] Pelupessy P, Duma L and Bodenhausen G 2008 *J. Magn. Reson.* **194** 169